Supplementary information: Addressing the exciton fine structure in colloidal nanocrystals: the case of CdSe nanoplatelets

Elena V. Shornikova, Louis Biadala, Dmitri R. Yakovlev, Victor F. Sapega, Yuri G. Kusrayev, Anatolie A. Mitioglu, Mariana V. Ballottin, Peter C. M. Christianen, Vasilii V. Belykh, Mikhail V. Kochiev, Nikolai N. Sibeldin, Aleksandr A. Golovatenko, Anna V. Rodina, Nikolay A. Gippius, Michel Nasilowski, Alexis Kuntzmann, Ye Jiang, Benoit Dubertret, and Manfred Bayer

S1. Band-edge exciton fine structure

It is well established theoretically and experimentally that in nanometer-sized colloidal semiconductor crystals the lowest eightfold degenerate exciton energy level is split into five fine structure levels by the intrinsic crystal field (in hexagonal lattice structures), the crystal shape asymmetry, and the electron-hole exchange interaction.[33,71] These levels are separated from each other by so large splitting energies, that at temperatures of a few Kelvin the photoluminescence (PL) arises from the two lowest exciton levels. In nearly spherical CdSe wurtzite QDs[29,31,32,34,51,72], as well as in zinc blende NPLs[27], the ground exciton state has total spin projection on the quantization axis $J = \pm 2$ and is forbidden in the electric-dipole (ED) approximation.§ Therefore, it is usually referred to as a "dark" state, $|F\rangle$. The upper lying "bright" state, $|A\rangle$, has $J = \pm 1^L$, and is ED allowed. The energy separation between these two levels $\Delta E_{\rm AF} = E_{\rm A} - E_{\rm F}$ is usually of the order of several meV and is relatively large compared to epitaxially grown quantum wells and quantum dots. These levels are schematically shown together with the relevant recombination and relaxation processes in Figure 4c.

Typically, the linewidth of ensemble PL spectra of colloidal nanocrystals is one-two orders of magnitude larger than the characteristic $\Delta E_{\rm AF} = 1 - 20$ meV. There are two optical methods that are commonly used to measure $\Delta E_{\rm AF}$ in different NCs.

1. Temperature-dependent time-resolved PL

The exciton fine structure leads to an interplay between the upper lying bright $|A\rangle$ and the lower dark $|F\rangle$ states that is typical for colloidal nanostructures. The recombination rates of these exciton states are $\Gamma_{\rm A}$ and $\Gamma_{\rm F}$. The PL intensity in this case can be written as $I(t) = \eta_{\rm A}\Gamma_{\rm A} p_{\rm A} + \eta_{\rm F}\Gamma_{\rm F} p_{\rm F}$, where $\eta_{\rm A,F}$ are the corresponding quantum efficiencies, and $p_{\rm A,F}$ are the occupation numbers of the corresponding levels. The relaxation rates between these levels are given by γ_0 and γ_{th}, where γ_0 is the zero-temperature relaxation rate from the bright to the dark exciton state, and $\gamma_{th} = \gamma_0 N_{\rm B}$ corresponds to the thermally-activated relaxation rate from the dark to the bright exciton state, where $N_{\rm B} = 1/\left[\exp(\Delta E_{\rm AF}/kT) - 1\right]$ is the Bose–Einstein phonon occupation. Assuming that γ_0, $\Gamma_{\rm A}$ and $\Gamma_{\rm F}$ are temperature independent parameters, the system dynamics can be described by the set of rate equations (1). The solutions of this system are:

$$\begin{aligned} p_{\rm A} &= C_1 e^{-t\Gamma_{\rm short}} + C_2 e^{-t\Gamma_{\rm L}}, \\ p_{\rm F} &= C_3 e^{-t\Gamma_{\rm short}} + C_4 e^{-t\Gamma_{\rm L}}, \end{aligned} \tag{S1}$$

with $\Gamma_{\rm short} = \tau_{\rm short}^{-1}$ and $\Gamma_{\rm L} = \tau_{\rm L}^{-1}$ being the rates for the short-lasting and the long-lasting decays, respectively:

$$\Gamma_{\rm short,L}(T) = \frac{1}{2}\left[\Gamma_{\rm A} + \Gamma_{\rm F} + \gamma_0 \coth\left(\frac{\Delta E_{\rm AF}}{2kT}\right) \pm \sqrt{(\Gamma_{\rm A} - \Gamma_{\rm F} + \gamma_0)^2 + \gamma_0^2 \sinh^{-2}\left(\frac{\Delta E_{\rm AF}}{2kT}\right)}\right], \tag{S2}$$

Here the sign "+" in front of the square root corresponds to $\Gamma_{\rm short}$ and the sign "–" to $\Gamma_{\rm L}$. For nonresonant excitation, after the laser pulse absorption, both $|A\rangle$ and $|F\rangle$ levels are assumed to be populated equally with $p_{\rm A}(t=0) = p_{\rm F}(t=0) = 0.5$, which gives:

$$\begin{aligned} p_{\rm A} &= C_1 e^{-t\Gamma_{\rm short}} + (0.5 - C_1) e^{-t\Gamma_{\rm L}}, \\ p_{\rm F} &= C_3 e^{-t\Gamma_{\rm short}} + (0.5 - C_3) e^{-t\Gamma_{\rm L}}. \end{aligned} \tag{S3}$$

Here C_1 and C_3 are temperature dependent parameters:

$$\begin{aligned} C_1 &= \frac{\gamma_0 + \Gamma_{\rm A} - \Gamma_{\rm L}}{2(\Gamma_{\rm short} - \Gamma_{\rm L})}, \\ C_3 &= \frac{-\gamma_0 + \Gamma_{\rm F} - \Gamma_{\rm L}}{2(\Gamma_{\rm short} - \Gamma_{\rm L})}. \end{aligned} \tag{S4}$$

§ In colloidal NCs, the exciton ground state is usually dark, with projection either ± 2 or $0^{\rm L}$, depending on the shape and/or crystal structure.

The PL intensity is then described by:

$$I(t) = [\eta_A \Gamma_A C_1 + \eta_F \Gamma_F C_3]\, e^{-t\Gamma_{short}} + [\eta_A \Gamma_A (0.5 - C_1) + \eta_F \Gamma_F (0.5 - C_3)]\, e^{-t\Gamma_L}. \quad \text{(S5)}$$

This dependence represents a bi-exponential PL decay, as typically observed in colloidal NCs at cryogenic temperatures. Indeed, after nonresonant photoexcitation and energy relaxation of excitons the bright and dark states at $t = 0$ are populated about equally, but only the emission from the bright exciton is observed due to $\Gamma_A \gg \Gamma_F$. In the limit $kT = 0$, the excitons relax to the $|F\rangle$ state with a rate γ_0. These two processes, namely, recombination of the bright exciton and relaxation to the dark state, result in a fast initial drop of the time-resolved PL with a rate $\Gamma_{short} = \Gamma_A + \gamma_0(1 + 2N_B) \approx \gamma_0(1 + 2N_B)$. At longer delays, the $|A\rangle$ level is emptied, and the emission arises from the $|F\rangle$ state with a rate $\Gamma_L = \Gamma_F$.

At a temperature of a few Kelvin, when $\Delta E_{AF} \gg kT$ the time-resolved PL is also bi-exponential with the decay rates Γ_{short} and Γ_L defined by equation (S2). When the temperature is increased, the short-lived (long-lived) component decelerates (accelerates). If $\gamma_0 \gg \Gamma_A$, at elevated temperatures corresponding to $\Delta E_{AF} \leq kT$ the decay turns into becoming mono-exponential with $\Gamma_L = (\Gamma_A + \Gamma_F)/2$ (see Figure 4a).

The temperature dependence of the Γ_L rate is therefore a powerful tool to measure the ΔE_{AF} value. At a single dot level, it has been shown that the energy splitting obtained by this method is in excellent agreement with the energy splitting directly measured from the PL spectra and also with theoretical calculations.[30] The analysis of the temperature dependence of the time-resolved PL decay is routinely used to evaluate ΔE_{AF} in NCs.[27,31,34,51,72,73] However, this method is indirect and might be affected by thermal activation of trap states,[34,51] surface dangling bonds,[35,36] as well as contributions from higher energy states.[73]

It is important to note, that typically in colloidal quantum dots $\gamma_0 \gg \Gamma_A$ so that the equations (2) can be simplified:[29]

$$\begin{aligned} \Gamma_{short} &= \Gamma_A + \gamma_0(1 + 2N_B) \approx \gamma_0(1 + 2N_B), \\ \Gamma_L(T) &= \frac{\Gamma_A + \Gamma_F}{2} - \frac{\Gamma_A - \Gamma_F}{2} \tanh\left(\frac{\Delta E_{AF}}{2kT}\right). \end{aligned} \quad \text{(S6)}$$

However, this simplification cannot be used in case of NPLs, where as we have shown in this paper Γ_A can be comparable with γ_0.

2. Fluorescence line narrowing

By exciting resonantly a small fraction of the NCs, the broadening due to the size distribution is drastically reduced and linewidths down to 300 μeV can be measured[28]. However, this method neglects any internal relaxation between the exciton states.[34] Moreover, it was shown recently that the Stokes shift in bare core CdSe QDs can be also contributed by formation of dangling bond magnetic polarons.[35] The FLN technique, therefore, may overestimate ΔE_{AF}.

S2. Sample characterization

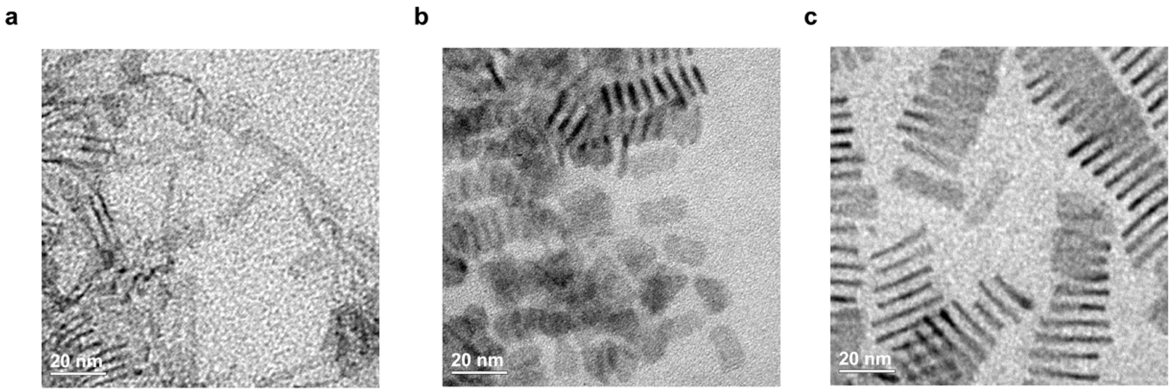

Fig. S1 TEM images of (a) 3ML, (b) 4ML, (c) 5ML CdSe NPLs.

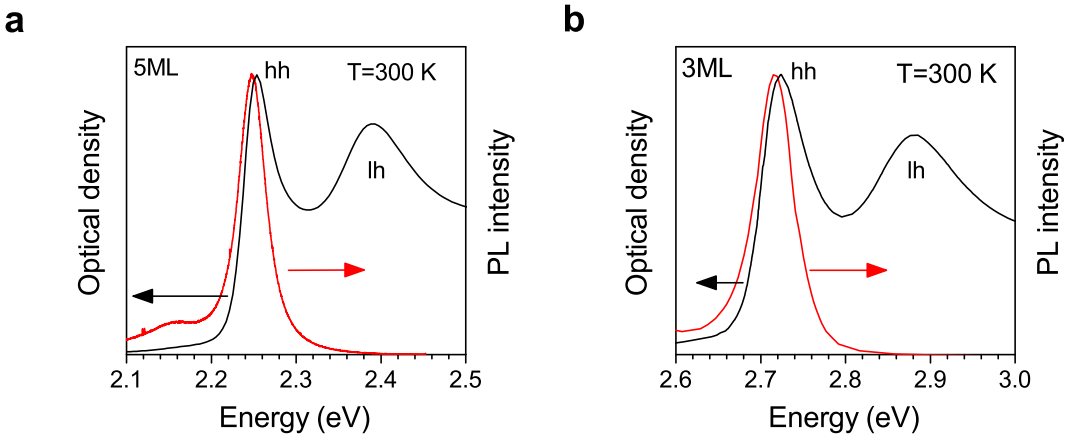

Fig. S2 Emission (red) and absorption (black) spectra of (a) 5ML and (b) 3ML CdSe NPLs measured at $T = 300$ K.

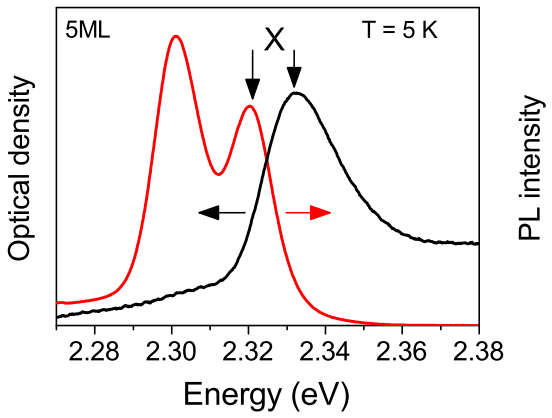

Fig. S3 Emission (red) and absorption (black) spectra of 5ML CdSe NPLs at $T = 5$ K. Exciton emission and absorption peaks are marked by arrows.

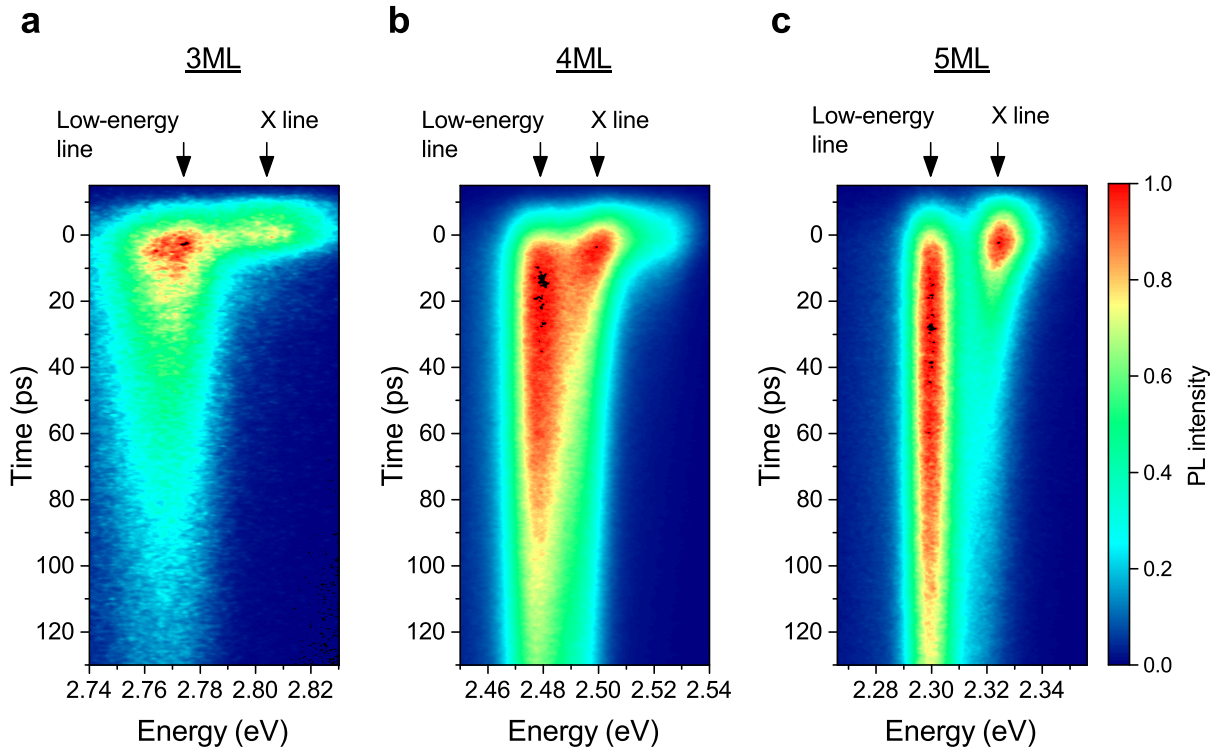

Fig. S4 Evolution of exciton and low-energy line emission of CdSe NPLs at $T = 2$ K measured with a streak-camera.

S3. Supplementary data for 5ML sample

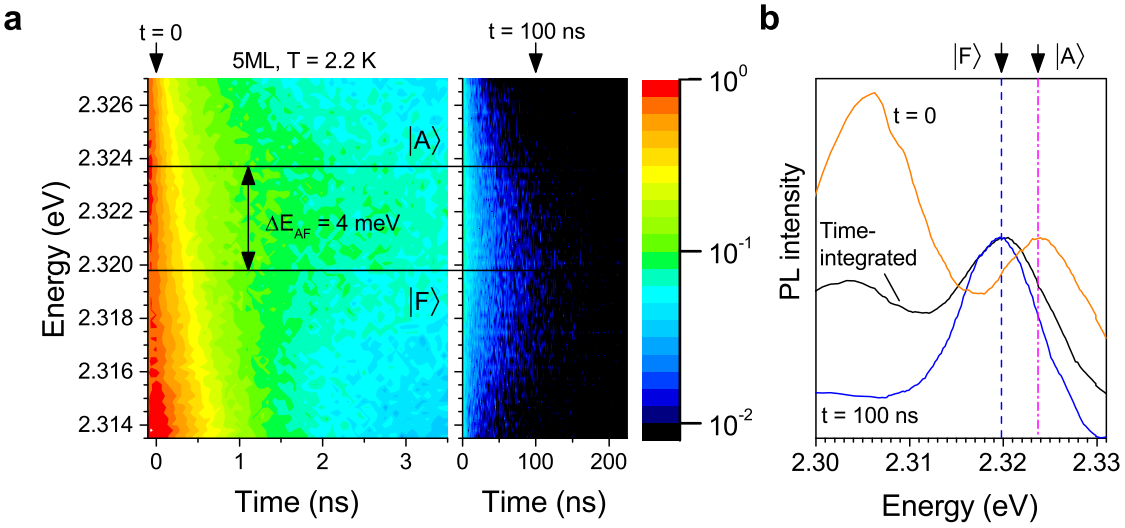

Fig. S5 (a) Spectrally-resolved PL decays of 5ML sample at $T = 2.2$ K shown for two temporal ranges. (b) PL spectra obtained by integration of the data in panel (a) over time at different delays: $t = 0$ (orange, integration range $-32 < t < 32$ ps), $t = 100$ ns (blue, integration range $95 < t < 105$ ns), and integrated over the whole period between subsequent laser pulses (black).

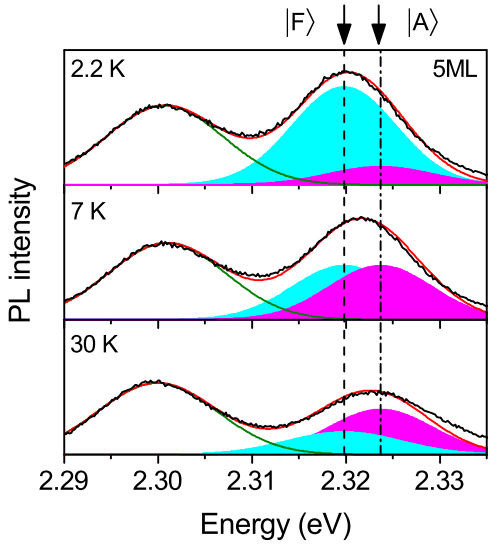

Fig. S6 PL spectra of 5ML sample at various temperatures. The data are fit with three Gaussians with the peak maxima corresponding to the bright exciton (magenta), dark exciton (cyan), and low-energy peak (green) positions. The fit results for I_F/I_A are presented in Figure 6b.

S4. "Method No. 5". Polarization-resolved PL spectra in magnetic fields

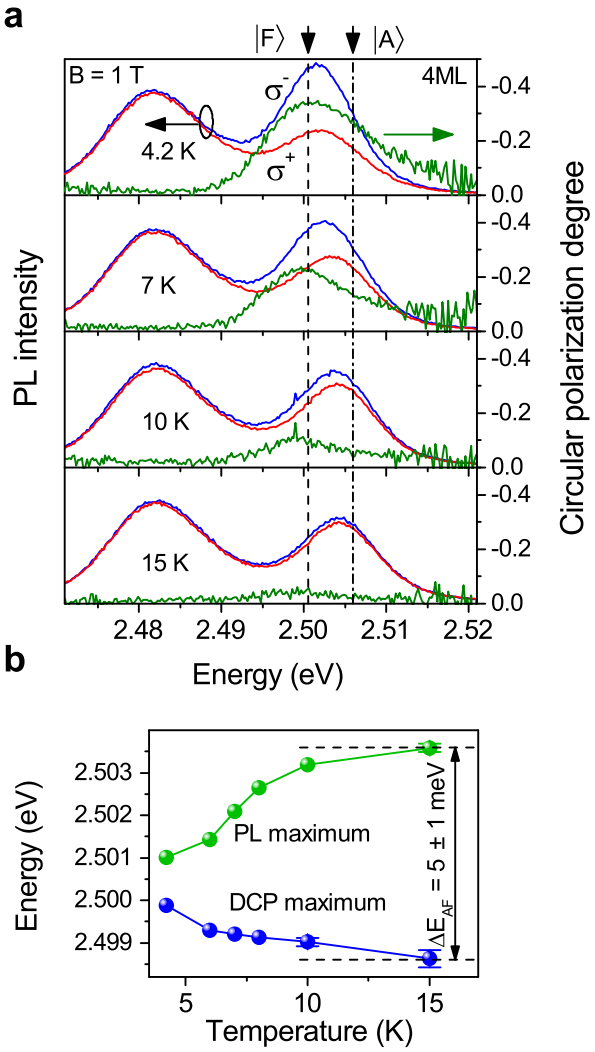

Fig. S7 (a) PL spectra of 4ML sample at various temperatures measured at $B = 1$ T. Left scale: intensity of σ^- (blue) and σ^+ (red) circularly polarized PL components. Right scale: degree of circular polarization. The spectral position of DCP maximum indicates the dark exciton energy E_F and does not shift with temperature (black dashed line). (b) Spectral position of the DCP maximum (blue) and PL maximum (green) versus temperature.

The circularly polarized emission in an external magnetic field can be also used for identification of the bright and dark excitons in colloidal NPLs. This method exploits the difference in the Zeeman splittings of the bright and dark excitons, which is controlled by their g-factors, g_X^A and g_X^F: $\Delta E_Z^{(A,F)}(B) = g_X^{(A,F)} \mu_B B \cos\theta$, where μ_B is the Bohr magneton and θ is the angle between the normal to the NPL plane and the magnetic field. Then the degree of circular polarization of the emission gained by the different thermal occupation of the exciton Zeeman sublevels is described by $P_c(B) = [\tau/(\tau+\tau_s)] \tanh[\Delta E_Z(B)/(2kT)]$. Here τ is exciton lifetime and τ_s is exciton spin relaxation time. The dark exciton state with angular momentum projection ± 2 has g-factor $g_X^F = g_e - 3g_h$.[33,74] While the bright exciton state with ± 1 has g-factor $g_X^A = -(g_e + 3g_h)$ for the case when the exchange interaction is smaller than the splitting between the light-hole and heavy-hole states, which is valid for NPL. One can see, that the g_X^F and g_X^A can differ considerably. The difference depends on g_e and g_h, which measurement for the studied NPLs goes beyond the scope of this paper.

A difference in g-factors has an immediate effect on the DCP by providing different values of $P_c(B)$ for the dark and bright excitons and different temperature dependences for them. This is confirmed by the experimental data in Fig. S7a, where the spectral dependence of the DCP is shown at $B = 1$ T and at temperatures varied from 4.2 to 15 K. With increasing temperature the absolute value of DCP decreases, but its maximum remains located at the spectral position of the dark exciton, while the PL maximum shifts with increasing temperature from the dark to bright exciton position (Fig. S7b). The energy difference between the DCP and PL maxima of about 5 meV at $T > 10$ K corresponds well with the ΔE_{AF} values for the 4ML NPLs (Table 3).

S5. Calculation of exciton parameters in c-CdSe NPL

In our calculations we consider only the contribution of the short-range electron-hole exchange interaction to the bright-dark exciton splitting $\Delta E_{\rm AF}$ in c-CdSe NPLs. We neglect its cubic anisotropy related to the contribution from remote bands to the Γ_8 valence band hole and write the isotropic electron-hole exchange Hamiltonian as:[33,62]

$$H_{\rm exch} = -\frac{2}{3}\varepsilon^{\rm c}_{\rm exch} a_{\rm c}^3 \delta(\boldsymbol{r}_{\rm e} - \boldsymbol{r}_{\rm h})(\boldsymbol{\sigma}\cdot\boldsymbol{J}), \tag{S7}$$

where $\varepsilon^{\rm c}_{\rm exch}$ is the exchange constant, $a_{\rm c} = 0.608$ nm is the lattice constant of c-CdSe[75], $\boldsymbol{\sigma} = (\sigma_x, \sigma_y, \sigma_z)$ is the Pauli matrix, and $\boldsymbol{J} = (J_x, J_y, J_z)$ is the matrix of the hole total angular momentum $J = 3/2$. We have found (see the main text) the resulting splitting as:

$$\Delta E_{\rm AF} = \Delta^{\rm c}_{\rm exch} |\tilde{\Psi}(0)|^2 / \tilde{L}, \tag{S8}$$

where $\tilde{L} = L/a_0$ is the dimensionless NPL thickness, $\tilde{\Psi}(0) = \Psi(0)a_0$ is the dimensionless in-plane wavefunction evaluated at $\rho_{\rm e} = \rho_{\rm h}$, and $\Delta^{\rm c}_{\rm exch} = \varepsilon^{\rm c}_{\rm exch} v_{\rm c}/a_0^3 = \varepsilon^{\rm c}_{\rm exch} a_{\rm c}^3/a_0^3$ is the renormalized exchange constant. Here we use $a_0 = 1$ nm as the length unit.

The influence of dielectric contrast on the in-plane wavefunction of exciton $\Psi(0)$ is taken into account according to approach described in Ref. [63]. The full Hamiltonian of the system includes potential $U_{e,h}(\rho, z_e, z_h)$ which describes the Coulomb attraction between electron and hole, the attraction of the electron to the hole image, and of the hole to the electron image. Potential $U_{e,h}(\rho, z_e, z_h)$ depends on $\varepsilon_{\rm out}$ and $\varepsilon_{\rm in}$ as follows:

$$U_{e,h}(\rho, z_e, z_h) = -\frac{e^2}{\varepsilon_{\rm in}}\left[\frac{1}{\sqrt{\rho^2 + (z_e - z_h)^2}} + \frac{\varepsilon_{\rm in} - \varepsilon_{\rm out}}{\varepsilon_{\rm in} + \varepsilon_{\rm out}} \frac{1}{\sqrt{\rho^2 + (z_e + z_h)^2}}\right], \tag{S9}$$

where $\rho = \rho_{\rm e} - \rho_{\rm h}$ is the exciton in-plane motion coordinate, z_e and z_h are coordinates of electron and hole along the quantization axis.

Let us consider the results of the $\Delta E_{\rm AF}$ calculations, performed for different sets of dielectric constants of the nanoplatelet $\varepsilon_{\rm in}$ and the surrounding media $\varepsilon_{\rm out}$. We consider four different values of renormalized exchange constant $\Delta^{\rm c}_{\rm exch}$.

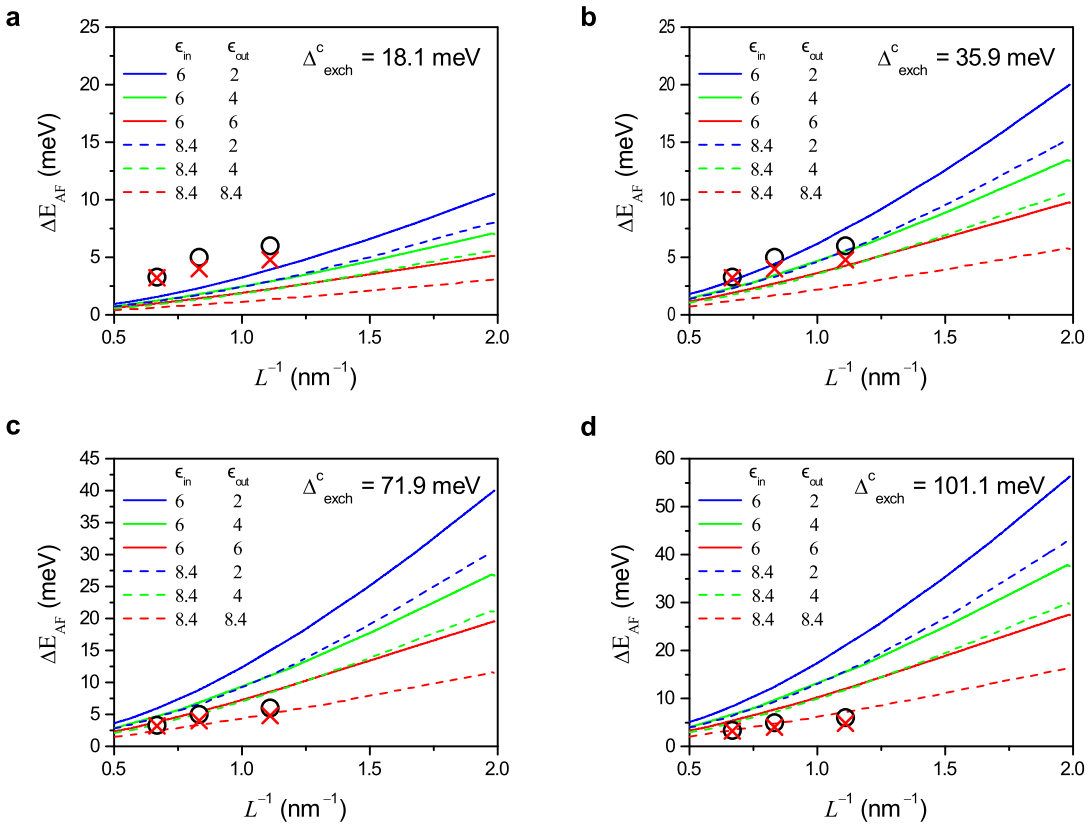

Fig. S8 Dependence of $\Delta E_{\rm AF}$ on NPL thickness for: (a) $\Delta^{\rm c}_{\rm exch} = 18.1$ meV, $\varepsilon^{\rm c}_{\rm exch} = 84$ meV (b) $\Delta^{\rm c}_{\rm exch} = 35.9$ meV, $\varepsilon^{\rm c}_{\rm exch} = 160$ meV, (c) $\Delta^{\rm c}_{\rm exch} = 71.9$ meV, $\varepsilon^{\rm c}_{\rm exch} = 320$ meV, and (d) $\Delta^{\rm c}_{\rm exch} = 101.1$ meV, $\varepsilon^{\rm c}_{\rm exch} = 450$ meV. Lines are calculations. Values of $\Delta E_{\rm AF}$ measured by FLN are shown by red crosses and values from temperature-dependent time-resolved PL are shown by black open circles.

a. The straightforward way to determine Δ^{c}_{exch} is based on the knowledge of the bright-dark splitting ΔE^{c}_{AF} in bulk c-CdSe (see Eq.7). However, there is no available experimental data for ΔE^{c}_{AF}. The empirical expression for the bulk exchange splitting in zinc-blende semiconductors was obtained in Ref. [76] from linear fit of splitting values in InP, GaAs and InAs. According to Eq.12 from Ref. [76] we find:

$$\Delta E^{c}_{AF}\left(\frac{a^{c}_{ex}}{a_0}\right)^3 = 15.4 \text{ meV}. \tag{S10}$$

It corresponds to the renormalized exchange constant $\Delta^{c}_{exch} = 18.1$ meV in c-CdSe, as well as in all other semiconductors with zincblende structure. Using the definition of c-CdSe unit cell from Refs. [78,79], we find $v_c = a_c^3 = 0.224$ nm^3, where $a_c = 0.608$ nm according to Ref. [75]. Therefore, $\Delta^{c}_{exch} = 18.1$ meV corresponds to the exchange constant $\varepsilon^{c}_{exch} = \Delta^{c}_{exch} a_0^3 / v_c = 69$ meV in c-CdSe. One can see that this choice of Δ^{c}_{exch} gives calculated ΔE_{AF} smaller than the experimental data at any ε_{in} and ε_{out} (Figure S8a).

b. The next approach is based on the assumption about equality of the renormalized exchange constants of c-CdSe and w-CdSe: $\Delta^{c}_{exch} = \Delta^{w}_{exch} = 35.9$ meV. The value of $\Delta^{c}_{exch} = 35.9$ meV corresponds to the $\varepsilon^{c}_{exch} = \Delta^{c}_{exch} a_0^3 / v_c = 160$ meV. This approach gives good agreement with the experimental results if we use ε_{in} varying from the high frequency dielectric constant of c-CdSe $\varepsilon_\infty = 6$ to the background dielectric constant of CdSe $\varepsilon_b = 8.4$, and the outside dielectric constant $\varepsilon_{out} = 2$. The results of calculations with the same Δ^{c}_{exch} and other sets of dielectric constants are presented in Fig. S8b.

c. Another approach is based on assumption about equality not of the renormalized exchange constants, but of the exchange constants ε_{exch} in c-CdSe and w-CdSe: $\varepsilon^{c}_{exch} = \varepsilon^{w}_{exch} = \Delta^{w}_{exch} {a_0}^3 / v_w = 320$ meV. Here $v_w = a_w^2 c_w \sqrt{3}/2 = 0.112$ nm^3 is the volume of the w-CdSe unit cell,[77] where $a_w = 0.43$ nm and $c_w = 0.70$ nm. From $v_c \approx 2v_w$ we obtain $\Delta^{c}_{exch} = 2\Delta^{w}_{exch} = 71.9$ meV. The choices $\varepsilon_{in} = 8.4$ and $\varepsilon_{out} = 4$ fit the experimental data (Fig. S8c).

d. The last approach is also based on assumption about equality of the exchange constants $\varepsilon^{c}_{exch} = \varepsilon^{w}_{exch}$ with the use of $\varepsilon^{w}_{exch} = 450$ meV from Ref. [33]. It gives us $\Delta^{c}_{exch} = \varepsilon^{c}_{exch} v_c / {a_0}^3 = 101.1$ meV. The calculated ΔE_{AF} is larger than the experimental data for any choice of ε_{in} and ε_{out}, except of the not very realistic case without a dielectric contrast: $\varepsilon_{in} = \varepsilon_{out} = 8.4$ (Figure S8d).

While we can exclude the cases without dielectric confinement, when $\varepsilon_{in} = \varepsilon_{out}$, and the cases with $\Delta^{c}_{exch} < 35.9$ meV, there are still a wide range of suitable parameterizations between those used in Figs. S8 b,c. Independent determination of the renormalized exchange constant Δ^{c}_{exch}, or dielectric constants ε_{in}, ε_{out} would allow one to narrow down the number of parameterizations. However, all these parameterizations use reasonable values of ε_{in}, ε_{out}, Δ^{c}_{exch} and allow us to describe dependence of bright-dark exciton splitting in c-CdSe NPLs as a result of short-range exchange interaction between electron and hole within the effective mass approximation approach.

References

1 C. B. Murray, D. J. Norris and M. G. Bawendi, *J. Am. Chem. Soc.*, 1993, **115**, 8706–8715.
2 S. Ithurria, M. D. Tessier, B. Mahler, R. P. S. M. Lobo, B. Dubertret and Al. L. Efros, *Nat. Mater.*, 2011, **10**, 936–941.
3 S. Ithurria and B. Dubertret, *J. Am. Chem. Soc.*, 2008, **130**, 16504–16505.
4 Y. Gao, M. C. Weidman and W. A. Tisdale, *Nano Lett.*, 2017, **17**, 3837–3843.
5 C. E. Rowland, I. Fedin, H. Zhang, S. K. Gray, A. O. Govorov, D. V. Talapin and R. D. Schaller, *Nat. Mater.*, 2015, **14**, 484–489.
6 J. Q. Grim, S. Christodoulou, F. Di Stasio, R. Krahne, R. Cingolani, L. Manna and I. Moreels, *Nat. Nanotechnol.*, 2014, **9**, 891–895.
7 B. T. Diroll, D. V. Talapin and R. D. Schaller, *ACS Photonics*, 2017, **4**, 576–583.
8 H.-T. Zhang,G. Wu and X.-H. Chen, *Langmuir*, 2005, **21**, 4281–4282.
9 C. Schliehe, B. H. Juarez, M. Pelletier, S. Jander, D. Greshnykh, M. Nagel, A. Meyer, S. Foerster, A. Kornowski, C. Klinke and H. Weller, *Science*, 2010, **329**, 550–553.
10 S. Dogan, T. Bielewicz, V. Lebedeva and C. Klinke, *Nanoscale*, 2015, **7**, 4875–4883.
11 M. Aerts, T. Bielewicz, C. Klinke, F. C. Grozema, A. J. Houtepen, J. M. Schins, and L. D. A.Siebbeles, *Nat. Commun.*, 2014, **5**, 3789.
12 J. Joo, J. S. Son, S. G. Kwon, J. H. Yu and T. Hyeon, *J. Am. Chem. Soc.*, 2006, **128**, 5632–5633.
13 J. S. Son, X.-D. Wen, J. Joo, J. Chae, S.-i. Baek, K. Park, J. H. Kim, K. An, J. H. Yu, S. G. Kwon, S.-H. Choi, Z. Wang, Y.-W. Kim, Y. Kuk, R. Hoffmann and T. Hyeon, *Angew. Chem., Int. Ed.*, 2009, **48**, 6861–6864.
14 Y.-H. Liu, V. L. Wayman, P. C. Gibbons, R. A. Loomis and W. E. Buhro, *Nano Lett.*, 2010, **10**, 352–357.
15 W.-k. Koh, N. K. Dandu, A. F. Fidler, V. I. Klimov, J. M. Pietryga and S. V. Kilina, *J. Am. Chem. Soc.*, 2017, **139**, 2152–2155.
16 M. B. Sigman, A. Ghezelbash, T. Hanrath, A. E. Saunders, F. Lee and B. A. Korgel, *J. Am. Chem. Soc.*, 2003, **125**, 16050–16057.
17 D. D. Vaughn II, R. J. Patel, M. A. Hickner and R. E. Schaak, *J. Am. Chem. Soc.*, 2010, **132**, 15170–15172.
18 Z. Li, H. Qin, D. Guzun, M. Benamara, G. Salamo and X. Peng, *Nano Research*, 2012, **5**, 337–351.
19 C. Bouet, D. Laufer, B. Mahler, B. Nadal, H. Heuclin, S. Pedetti, G. Patriarche and B. Dubertret, *Chem. Mater.*, 2014, **26**, 3002–3008.
20 E. Izquierdo, A. Robin, S. Keuleyan, N. Lequeux, E. Lhuillier and S. Ithurria, *J. Am. Chem. Soc.*, 2016, **138**, 10496–10501.
21 M. Nasilowski, B. Mahler, E. Lhuillier, S. Ithurria and B. Dubertret, *Chem. Rev.*, 2016, **116**, 10934–10982.
22 A. Yeltik, S. Delikanli, M. Olutas, Y. Kelestemur, B. Guzelturk and H. V. Demir, *J. Phys. Chem. C*, 2015, **119**, 26768–26775.

23 A. W. Achtstein, A. Antanovich, A. Prudnikau, R. Scott, U. Woggon and M. Artemyev, *J. Phys. Chem. C*, 2015, **119**, 20156–20161.

24 E. Cassette, R. D. Pensack, B. Mahler and G. D. Scholes, *Nature Commun.*, 2015, **6**, 6086.

25 S. Pal, P. Nijjar, T. Frauenheim and O. V. Prezhdo, *Nano Lett.*, 2017, **17**, 2389–2396.

26 R. Benchamekh, N. A. Gippius, J. Even, M. O. Nestoklon, J.-M. Jancu, S. Ithurria, B. Dubertret, Al. L. Efros and P. Voisin, *Phys. Rev. B*, 2014, **89**, 035307.

27 L. Biadala, F. Liu, M. D. Tessier, D. R. Yakovlev, B. Dubertret and M. Bayer, *Nano Lett.*, 2014, **14**, 1134–1139.

28 A. Granados Del Águila, B. Jha, F. Pietra, E. Groeneveld, C. De Mello Donegá, J. C. Maan, D. Vanmaekelbergh and P. C. M. Christianen, *ACS Nano*, 2014, **8**, 5921–5931.

29 O. Labeau, P. Tamarat and B. Lounis, *Phys. Rev. Lett.*, 2003, **90**, 257404.

30 L. Biadala, Y. Louyer, P. Tamarat and B. Lounis, *Phys. Rev. Lett.*, 2009, **103**, 037404.

31 S. Brovelli, R. D. Schaller, S. A. Crooker, F. García-Santamaría, Y. Chen, R. Viswanatha, J. A. Hollingsworth, H. Htoon and V. I. Klimov, *Nat. Commun.*, 2011, **2**, 280.

32 M. Nirmal, D. Norris, M. Kuno, M. Bawendi, Al. L. Efros and M. Rosen, *Phys. Rev. Lett.*, 1995, **75**, 3728–3731.

33 Al. L. Efros, M. Rosen, M. Kuno, M. Nirmal, D. Norris and M. Bawendi, *Phys. Rev. B*, 1996, **54**, 4843–4856.

34 C. De Mello Donegá, M. Bode and A. Meijerink, *Phys. Rev. B*, 2006, **74**, 085320.

35 L. Biadala, E. V. Shornikova, A. V. Rodina, D. R. Yakovlev, B. Siebers, T. Aubert, M. Nasilowski, Z. Hens, B. Dubertet, Al. L. Efros and M. Bayer, *Nat. Nanotechnol.*, 2017, **12**, 569–574.

36 A. Rodina and Al. L. Efros, *Nano Lett.*, 2015, **15**, 4214–4222.

37 K. Leung, S. Pokrant and K. B. Whaley, *Phys. Rev. B*, 1998, **57**, 12291–12301.

38 Z. Li and X. Peng *J. Am. Chem. Soc.* 2011, **133**, 6578–6586.

39 Ch. She, I. Fedin, D. S. Dolzhnikov, A. Demortière, R. D. Schaller, M. Pelton and D. V. Talapin, *Nano Lett.*, 2014, **14**, 2772–2777.

40 D. Chen, Y. Gao, Y. Chen, Y. Ren and X. Peng, *Nano Lett.*, 2015, **15**, 4477–4482.

41 M. D. Tessier, C. Javaux, I. Maksimovic, V. Loriette and B. Dubertret, *ACS Nano*, 2012, **6**, 6751–6758.

42 D. C. Hannah, N. J. Dunn, S. Ithurria, D. V. Talapin, L. X. Chen, M. Pelton, G. C. Schatz and R. D. Schaller, *Phys. Rev. Lett.*, 2011, **107**, 177403.

43 M. D. Tessier, L. Biadala, C. Bouet, S. Ithurria, B. Abecassis and B. Dubertret, *ACS Nano*, 2013, **7**, 3332–3340.

44 A. W. Achtstein, R. Scott, S. Kickhöfel, S. T. Jagsch, S. Christodoulou, G. H. V. Bertrand, A. V. Prudnikau, A. Antanovich, M. Artemyev, I. Moreels, A. Schliwa and U. Woggon, *Phys. Rev. Lett.*, 2016, **116**, 116802.

45 O. Erdem, M. Olutas, B. Guzelturk, Y. Kelestemur and H. V. Demir, *J. Phys. Chem. Lett.*, 2016, **7**, 548–554.

46 S. A. Cherevkov, A. V. Fedorov, M. V. Artemyev, A. V. Prudnikau and A. V. Baranov, *Phys. Rev. B*, 2013, **88**, 041303R.

47 V. Dzhagan, A. G. Milekhin, M. Ya. Valakh, S. Pedetti, M. Tessier, B. Dubertret and D. R. T. Zahn, *Nanoscale*, 2016, **8**, 17204.

48 F. Liu, L. Biadala, A. V. Rodina, D. R. Yakovlev, D. Dunker, C. Javaux, J. P. Hermier, Al. L. Efros, B. Dubertret and M. Bayer, *Phys. Rev. B*, 2013, **88**, 035302.

49 M. Furis, H. Htoon, M. A. Petruska, V. I. Klimov, T. Barrick and S. A. Crooker, *Phys. Rev. B*, 2006, **73**, 241313R.

50 F. J. P. Wijnen, J. H. Blokland, P. T. K. Chin, P. C. M. Christianen and J. C. Maan, *Phys. Rev. B*, 2008, **78**, 235318.

51 S. A. Crooker, T. Barrick, J. A. Hollingsworth and V. I. Klimov, *Appl. Phys. Lett.*, 2003, **82**, 2793.

52 V. A. Kiselev, B. S. Razbirin and I. N. Uraltsev, *Phys. Status Solidi B*, 1975, **72**, 161–172.

53 V. P. Kochereshko, G. V. Mikhailov and I. N. Uraltsev, *Sov. Phys. Solid State*, 1983 **25**, 439. [transl. *Fiz. Tverd. Tela*, 1983, **25**, 769–776.]

54 Y. Louyer, L. Biadala, J. B. Trebbia, M. J. Fernée, P. Tamarat and B. Lounis, *Nano Lett.*, 2011, **11**, 4370–4375.

55 A. Naeem, F. Masia, S. Christodoulou, I. Moreels, P. Borri and W. Langbein, *Phys. Rev. B*, 2015, **91**, 121302(R).

56 B. Segall and D. T. F. Marple, *Physics and Chemistry of II–VI Compounds*, eds. M. Aven and J. S. Prener, North Holland, Amsterdam, 1967, p. 317.

57 S. Shionoya, *Proc. 12th Int. Conf. Phys. Semicond.*, Stuttgart, Germany, 1974, 113.

58 J. Voigt, F. Spiegelberg and M. Senoner, *Phys. Status Solidi (b)*, 1979, **91**, 189.

59 J. M. Elward and A. Chakraborty, *J. Chem. Theory Comput.*, 2013, **9**, 4351–4359.

60 M. Nirmal, C. Murray and M. Bawendi *Phys. Rev. B*, 1994, **50**, 2293–2300.

61 C. R. L. P. N. Jeukens, P. C. M. Christianen, J. C. Maan, D. R. Yakovlev, W. Ossau, V. P. Kochereshko, T. Wojtowicz, G. Karczewski and J. Kossut, *Phys. Rev. B*, 2002, **66**, 235318.

62 E.L. Ivchenko and G.E. Pikus, *Superlattices and other heterostuctures. Symmetry and optical properties*, Springer, Berlin, 2nd edn, 1997, p. 159.

63 N. A. Gippius, A. L. Yablonskii, A. B. Dzyubenko, S. G. Tikhodeev, L. V. Kulik, V. D. Kulakovskii and A. Forchel, *J. Appl. Phys.*, 1998,

83, 5410–5417.
64 A. Pawlis, T. Berstermann, C. Brüggemann, M. Bombeck, D. Dunker, D. R. Yakovlev, N. A. Gippius, K. Lischka and M. Bayer, *Phys. Rev. B*, 2011, **83**, 115302.
65 M. Cardona and R. G. Ulbrich, *Light Scattering in Solids III*, Springer, Berlin, 2005, Topics in Applied Physics, vol. 51, p. 233.
66 A. V. Rodina and Al. L. Efros, *JETP*, 2016, **122**, 554–556.
67 M. D. Lechner, *Refractive Indices of Organic Liquids*, Springer, Berlin, 1996, Group III, vol. 38B.
68 J. Feldmann, G. Peter, E. O. Göbel, P. Dawson, K. Moore, C. Foxon and R. J. Elliott, *Phys. Rev. Lett.*, 1987, **59**, 2337–2340.
69 A. Polhmann, R. Hellmann, E. O. Göbel, D. R. Yakovlev, W. Ossau, A. Waag, R. N. Bicknell-Tassius and G. Landwehr, *Appl. Phys. Lett.*, 1992, **61**, 2929–2931.
70 F. Gindele, U. Woggon, W. Langbein, J. M. Hvam, M. Hetterich and C. Klingshirn, *Solid State Commun.*, 1998, **106**, 653–657.
71 A. V. Rodina and Al. L. Efros, *Phys. Rev. B*, 2016, **93**, 155427.
72 L. Biadala, Y. Louyer, P. Tamarat and B. Lounis, *Phys. Rev. Lett.*, 2010, **105**, 157402.
73 L. Biadala, B. Siebers, Y. Beyazit, M. D. Tessier, D. Dupont, Z. Hens, D. R. Yakovlev and M. Bayer, *ACS Nano*, 2016, **10**, 3356–3364.
74 Al. L. Efros in *Semiconductor and Metal Nanocrystals: Synthesis and Electronic and Optical Properties*, ed. V. I. Klimov, Dekker, New York, 2003, ch. 3, pp. 103–141.
75 N. Samarth, H. Luo, J. K. Furdyna, S. B. Qadri, Y. R. Lee, A. K. Ramdas and N. Otsuka, *Appl. Phys. Lett.*, 1989, **54** 2680–2682.
76 H. Fu, L.W. Wang and A. Zunger, *Phys. Rev. B*, 1999 **59**, 5568.
77 Y.-N. Xu and W. Y. Ching, *Phys. Rev. B*, 1993, **48**, 4335–4351.
78 Z. Zarhri, A. Abassi, H. Ez. Zahraouy, Y. El. Amraoui, A. Benyoussef and A. El. Kenz, *J. Supercond. Nov. Magn.*, 2015, **28**, 2155–2160.
79 A. Szemjonov, T. Pauporté, I. Ciofini and F. Labat, *Phys. Chem. Chem. Phys.*, 2014 **16**, 23251.